

Infrared Narrow-Band Tomography of the Local Starburst NGC 1569 with LBT/LUCIFER

A. Pasquali¹, A. Bik, S. Zibetti²

Max-Planck Institut für Astronomie, Königstuhl 17, 69117 Heidelberg, Germany

N. Ageorges

Max-Planck-Institut für extraterrestrische Physik, Giessenbachstrasse, 85748 Garching,
Germany

W. Seifert

Landessternwarte Heidelberg, Königstuhl, 69117 Heidelberg, Germany

W. Brandner, H.-W. Rix

Max-Planck-Institut für Astronomie, Königstuhl 17, 69117 Heidelberg, Germany

M. Jütte, V. Knierim

Ruhr-Universität, Universitätstrasse 150, 44780 Bochum, Germany

P. Buschkamp

Max-Planck-Institut für extraterrestrische Physik, Giessenbachstrasse, 85748 Garching,
Germany

C. Feiz

Landessternwarte Heidelberg, Königstuhl, 69117 Heidelberg, Germany

H. Gemperlein

Max-Planck-Institut für extraterrestrische Physik, Giessenbachstrasse, 85748 Garching,
Germany

A. Germeroth

Landessternwarte Heidelberg, Königstuhl, 69117 Heidelberg, Germany

R. Hofmann

Max-Planck-Institut für extraterrestrische Physik, Giessenbachstrasse, 85748 Garching,
Germany

W. Laun

Max-Planck Institut für Astronomie, Königstuhl 17, 69117 Heidelberg, Germany

R. Lederer

Max-Planck-Institut für extraterrestrische Physik, Giessenbachstrasse, 85748 Garching,
Germany

M. Lehmitz, R. Lenzen, U. Mall

Max-Planck-Institut für Astronomie, Königstuhl 17, 69117 Heidelberg, Germany

H. Mandel, P. Müller

Landessternwarte Heidelberg, Königstuhl, 69117 Heidelberg, Germany

V. Naranjo

Max-Planck-Institut für Astronomie, Königstuhl 17, 69117 Heidelberg, Germany

K. Polsterer

Ruhr-Universität, Universitätstrasse 150, 44780 Bochum, Germany

A. Quirrenbach, L. Schäffner

Landessternwarte Heidelberg, Königstuhl, 69117 Heidelberg, Germany

C. Storz

Max-Planck-Institut für Astronomie, Königstuhl 17, 69117 Heidelberg, Germany

P. Weiser

Fachhochschule für Technik und Gestaltung, Speyerer Strasse 4, 68163 Mannheim,
Germany

Received _____; accepted _____

¹Astronomisches Rechen Institut, Mönchhofstrasse 12 - 14, 69120 Heidelberg, Germany

²Dark Cosmology Centre, Niels Bohr Institute - University of Copenhagen, Juliane Maries
Vej 30, DK-2100 Copenhagen, Denmark

ABSTRACT

We used the near-IR imager/spectrograph LUCIFER mounted on the Large Binocular Telescope (LBT) to image, with sub-arcsec seeing, the local dwarf starburst NGC 1569 in the JHK bands and HeI $1.08\mu\text{m}$, [FeII] $1.64\mu\text{m}$ and Br γ narrow-band filters. We obtained high-quality spatial maps of HeI $1.08\mu\text{m}$, [FeII] $1.64\mu\text{m}$ and Br γ emission across the galaxy, and used them together with *HST*/ACS images of NGC 1569 in the H α filter to derive the two-dimensional spatial map of the dust extinction and surface star formation rate density. We show that dust extinction (as derived from the H α /Br γ flux ratio) is rather patchy and, on average, higher in the North-West (NW) portion of the galaxy [$E_g(\text{B-V}) \simeq 0.71$ mag] than in the South-East [$E_g(\text{B-V}) \simeq 0.57$ mag]. Similarly, the surface density of star formation rate (computed from either the dereddened H α or dereddened Br γ image) peaks in the NW region of NGC 1569, reaching a value of about $4 \times 10^{-6} \text{ M}_\odot \text{ yr}^{-1} \text{ pc}^{-2}$. The total star formation rate as estimated from the integrated, dereddened H α (or, alternatively, Br γ) luminosity is about $0.4 \text{ M}_\odot \text{ yr}^{-1}$, and the total supernova rate from the integrated, dereddened [FeII] $1.64\mu\text{m}$ luminosity is about 0.005 yr^{-1} (assuming a distance of 3.36 Mpc). The azimuthally averaged [FeII] $1.64\mu\text{m}$ /Br γ flux ratio is larger at the edges of the central, gas-deficient cavities (encompassing the super star clusters A and B) and in the galaxy outskirts. If we interpret this line ratio as the ratio between the average past star formation (as traced by supernovae) and on-going activity (represented by OB stars able to ionize the interstellar medium), it would then indicate that star formation has been quenched within the central cavities and lately triggered in a ring around them. The number of ionizing hydrogen and helium photons as computed from the integrated, dereddened H α and HeI $1.08\mu\text{m}$ luminosities suggests that the latest burst of star formation occurred about 4

Myr ago and produced new stars with a total mass of $\simeq 1.8 \times 10^6 M_{\odot}$.

Subject headings: galaxies: dwarf — galaxies: individual (NGC 1569) — galaxies: irregular — galaxies: starburst — galaxies: star formation

1. Introduction

Understanding the star formation activity and history of local dwarf galaxies is of high astrophysical relevance. In fact, they represent ideal laboratories to study how star formation occurs in low-metallicity environments that, at the same time, do not show any global, ordered kinematic structure as in disk galaxies. As such, dwarf galaxies allow us to study how stellar feedback alone affects the physics, kinematics and chemical enrichment of the interstellar medium. Nearby, star-forming dwarf galaxies that are metal-poor and gas-rich are often compared to the first galaxies in the early Universe (see Izotov & Thuan 1999), which were the first structures to collapse from primordial density fluctuations, and gave rise to larger systems through mergers (White & Frenk 1991; Kauffmann, White & Guiderdoni 1993; Cole et al. 1994). They are also referred to as the possible local counterparts of starbursting galaxies that, at moderate redshift, dominate the faint galaxy counts at blue wavelengths (Broadhurst, Ellis & Glazebrook 1992; Lilly et al. 1995).

The nearby galaxy NGC 1569 is considered to be the archetype starburst dwarf galaxy for several reasons. First of all, it is gas-rich and relatively metal-poor: at the revised distance of 3.36 Mpc (Grocholski et al. 2008, so that $M_B = -18$), its HI and dynamical masses are $\sim 2 \times 10^8 M_\odot$ and $5.1 \times 10^8 M_\odot$, respectively (adapted from Reakes 1980). Its gas-phase and stellar metallicities are estimated to be $12 + \log(\text{O}/\text{H}) \simeq 8.3$ (Calzetti, Kinney & Storchi-Bergmann 1994; González Delgado et al. 1997, Kobulnicky & Skillman 1997) and $Z \sim 0.1 - 0.2 Z_\odot$ (Grocholski et al. 2008; Aloisi et al. 2001), respectively. Star formation has taken place in NGC 1569 for a Hubble time, although with different intensities as obtained by Vallenari & Bomans (1996), Greggio et al. (1998), Aloisi et al. (2001) and Angeretti et al. (2005) using color-magnitude diagrams of resolved stars. The recent studies by Angeretti et al. (2005) and Grocholski et al. (2008) show that the star formation activity of NGC 1569 started about 10 Gyr ago and proceeded until ~ 1 Gyr ago

presumably at a constant, very low rate. In the last 1 Gyr, however, NGC 1569 experienced at least three major bursts of star formation: *i*) the older one started about 1 Gyr ago and ended ~ 100 Myr ago with an average star formation rate ($\langle \text{SFR} \rangle$) of about $0.04 M_{\odot} \text{ yr}^{-1}$; *ii*) the intermediate episode was triggered about ~ 100 Myr ago and lasted up to 30 Myr ago with $\langle \text{SFR} \rangle \sim 0.08 M_{\odot} \text{ yr}^{-1}$, and *iii*) the younger burst began ~ 27 Myr ago and ended about 8 Myr ago with $\langle \text{SFR} \rangle \sim 0.3 M_{\odot} \text{ yr}^{-1}$ (Angeretti et al. 2005). According to Aloisi et al. (2001), the spatial distribution of stars across the galaxy changes with their age, so that stars younger than 50 Myr are more centrally concentrated, intermediate age stars (50 Myr - 1 Gyr) are uniformly distributed, and older stars are mostly found in the outskirts of NGC 1569. Angeretti et al. (2005) suggested that this episodic star formation (in the last 1 Gyr) could be ascribed to the gravitational interactions of NGC 1569 with an HI cloud ($\sim 7 \times 10^6 M_{\odot}$ in mass) a few kpc away yet connected to the galaxy by an HI bridge (cf. Stil & Israel 1998).

The presence of several HII regions (Waller 1991) and the spatially extended $\text{H}\alpha$ emission indicate that NGC 1569 has formed new stars rather recently. Hunter & Elmegreen (2004) used the spatially integrated $\text{H}\alpha$ luminosity (corrected for reddening) to derive a SFR of $\sim 0.6 M_{\odot} \text{ yr}^{-1}$ (adjusted to a distance of 3.36 Mpc). The morphology of the extended $\text{H}\alpha$ is rather complex and characterized by arcs, filaments and four large-scale superbubbles (Hunter et al. 1993; Heckman et al. 1995; Martin 1998; Westmoquette et al. 2008). The latter are seen to expand at typical velocities of $\sim 100 \text{ km s}^{-1}$ which imply dynamical ages < 25 Myr, consistent with the most recent burst of star formation derived by Angeretti et al. (2005; Heckman et al. 1995; Westmoquette, Smith & Gallagher 2008). The expansion of these superbubbles is most likely powering a galactic outflow throughout the disk whose direction is approximately perpendicular to the inclined and flattened HI disc of NGC 1569. The presence of an outflow of ionized gas is also supported by the high $[\text{SII}]/\text{H}\alpha$ ratios measured within the superbubbles and indicative of shocks (Westmoquette,

Smith & Gallagher 2008). The arcs of ionized gas detected in $H\alpha$ and X-ray in the superbubbles suggest that the hot gas is still confined within the superbubbles, although it is moving at the escape velocity of NGC 1569. Thus, at present day, the galactic outflow of NGC 1569 does not appear to be in a steady state and to be able to induce mass loss from the galaxy (Westmoquette, Smith & Gallagher 2008).

NGC 1569 is special also for another reason: it hosts two of the nearest super-star clusters known (SSCs A and B, Arp & Sandage 1985). SSCs are massive star clusters few Myr to several hundred Myr old, believed to be the ancestors of globular clusters. In fact, they are as extended and massive as globular clusters and, after ~ 10 Gyr of passive evolution, they can match the luminosity range spanned by globular clusters today (cf. van den Bergh 1995; Meurer 1995). They are typically observed in interacting/merger systems (see Whitmore et al. 1993) and starburst galaxies (see Meurer et al. 1995). In NGC 1569, SSC A has been resolved into two components (A1 and A2, De Marchi et al. 1997), of which A2 may be the host of young O and Wolf-Rayet stars and A1 together with SSC B may be dominated by older red supergiants (Origlia et al. 2001). González Delgado et al. (1997) suggested that SSCs A and B have possibly undergone sequential star formation, with two major bursts of star formation about 3 and 9 Myr ago. The authors also found a deficit of ionized gas around SSCs A and B which may have been created by the stellar winds and supernova explosions of the older burst removing the local gas. According to the measurements of Ho & Filippenko (1996) SSC A is as massive as $\sim 4 \times 10^5 M_{\odot}$ (adjusted to a distance of 3.36 Mpc).

Age dating of star clusters and resolved stars strongly depends on dust extinction. Studies of the stellar content of NGC 1569 based on long-slit spectroscopy show that the intrinsic dust extinction varies across NGC 1569 by few tenths of a dex, and peaks at SSCs A and B (González Delgado et al. 1997; Origlia et al. 2001) and in the North-West portion of

the galaxy (Kobulnicky & Skillman 1997). The spatial coverage of long-slit spectroscopy is coarse, however, and no uniform and contiguous two-dimensional map of the dust extinction in NGC 1569 is available in the literature. Clearly, such a 2D map helps in reaching a higher accuracy in the determination of the star formation history and its associated star formation rate across NGC 1569. For this reason, we have taken advantage of the large field of view of LUCIFER (LBT NIR spectroscopic Utility with Camera and Integral-Field Unit for Extragalactic Research) mounted on the Large Binocular Telescope (LBT) to perform deep imaging in the Br γ filter and in the K band. Our aim is to construct the 2D spatial map of dust extinction across NGC 1569 from the Br γ and H α (obtained with the Advanced Camera for Surveys on HST) images of the galaxy and to derive the 2D spatial distribution of star formation rate density. We also observed the HeI 1.08 μ and [FeII] 1.64 μ lines and their broad-band continua in order to estimate the number of massive young stars and the supernova rate in NGC 1569, respectively. The observations and data reduction are described in Sect. 2. The spatial distribution of the color excess $E_g(B-V)$ associated with the gas and the spatial distribution of the star formation rate density across NGC 1569 are derived in Sect. 3 and 4, respectively, while the properties of the [FeII] 1.64 μ m emission are analyzed in Sect. 5. Conclusions follow in Sect. 6.

2. Observations

The observations presented here were carried out with the LBT, located on Mount Graham, Arizona (Hill, Green & Slagle 2006). NGC 1569 was observed during the science commissioning of LUCIFER (Ageorges et al. 2010; Seifert et al. 2010), with the N3.75 camera which provides a 4' \times 4' field of view at an angular resolution of 0.12"/pixel (equivalent to 1.95 pc per pixel at the adopted distance of 3.36 Mpc). We imaged NGC 1569 between September and November 2009 in the JHK broad bands and in the narrow-band

HeI $1.08\mu\text{m}$, [FeII] $1.64\mu\text{m}$ and Br γ filters, with a seeing $\leq 0.5''$ (i.e. 8 pc) throughout the observing runs. Although the exposure times in the broad-band and Br γ filters were estimated from the available 2MASS photometry and *HST*/ACS F658N ($\text{H}\alpha$) image via the LUCIFER Exposure Time Calculator, the effective exposure times were largely dictated by the available amount of time during the LUCIFER commissioning. The exposure time for each of the HeI $1.08\mu\text{m}$ and [FeII] $1.64\mu\text{m}$ filters was initially set to 1 hour (following Labrie & Pritchett 2006), but it was later cut down to 30 min for the HeI $1.08\mu\text{m}$. The final exposure times on source achieved for the near-IR dataset are listed in Table 1, together with the imaging taken in the F606W (broad V) and F658N ($\text{H}\alpha$) filters with *HST*/ACS as part of program ID 10885 (PI Aloisi).

The near-IR images were reduced with standard IRAF¹ routines. They were corrected for bias and flat-fielding, and their astrometric solution was derived from the field stars in common with 2MASS. After background subtraction, the images taken in the same filter were corrected for geometric distortion and then combined together on the basis of their World Coordinate System with a weighted mean. The final mosaiced frames in the broad band filters were flux-calibrated, at a 10% accuracy, using the 2MASS magnitudes of the stars in the field of NGC 1569.

After convolution to the same PSF (FWHM = $0.5''$) the continuum emission was subtracted from each narrow-band image by scaling the closest broad-band image (J for HeI $1.08\mu\text{m}$, H for [FeII] $1.64\mu\text{m}$ and K for Br γ) so that field stars would have had the same integrated count rate in both the narrow and broad band filters. This scaling was applied to the broad band zero points in order to calibrate the pure emission line images in flux, with an achieved

¹IRAF is distributed by the National Optical Astronomy Observatory, which is operated by the Association of Universities for Research in Astronomy, Inc., under cooperative agreement with the National Science Foundation.

accuracy of 20% (estimated from the scatter in the zero point derived from different stars).

The optical HST/ACS images were retrieved from the HST archive already reduced. The subtraction of the continuum emission (the F606W image) from the F658N frame and the flux calibration of the pure H α emission were performed as for the near-IR data, reaching a flux accuracy of 20%. Such a low accuracy in the flux calibration of the H α is mostly due to the broad F606W filter which makes it impossible to account for color terms. The H α -emission image was corrected for a 5% flux contribution from the [NII] λ 6548,6584 lines (Moustakas & Kennicutt 2006), and then convolved with a Gaussian function to have the same stellar PSF as the Br γ -emission image, resampled to achieve the same pixel scale as the LUCIFER N3.75 camera, and aligned to the Br γ -emission image.

Most of the analysis presented in the following sections requires or involves the production of spatially resolved maps of flux ratios in different passbands. In order to ensure a sufficient S/N for the largest number of pixels while retaining the best possible spatial resolution, we adopt the approach introduced by Zibetti, Charlot & Rix (2009) using the adaptive smoothing code ADAPTSMOOTH (Zibetti 2009). We first smooth each image individually by taking the median flux among the pixels inside a top-hat circular kernel, whose size is determined as the minimum that allows to obtain a $S/N \geq 10$ (background dominated noise is assumed). The spatial match between different bands is obtained by requiring that the kernel size at each pixel location ensures a minimum S/N of 10 in all images (see Zibetti 2009 for details). The smoothing procedure also results in a first S/N cut: all pixels for which sufficient S/N of 10 cannot be reached in all images even when the maximum kernel size of 27 pixels is used are flagged. A further S/N cut is applied by excluding all pixels whose flux (in the smoothed image) is less than 3σ of the large scale background fluctuations as measured from randomly placed boxes of a few hundred pixels on a side.

3. The spatial map of dust extinction

The line-emission images of NGC 1569 are shown in Fig. 1, already flux-calibrated but not corrected for dust extinction. Fluxes, in units of $\text{erg cm}^{-2} \text{s}^{-1}$, are displayed in logarithmic scale across an area of $1.5 \text{ kpc} \times 1 \text{ kpc}$ at the adopted distance of 3.36 Mpc. We clearly detect the base of the north-western arm as well as “cavities” at the center of the galaxy where SSCs A and B reside, and corresponding to the cluster surroundings where González Delgado et al. (1997) found a deficit of ionized gas. These regions were flagged as underflow pixels by our smoothing procedure. The S/N cut used in our image smoothing results in a limiting flux of $\approx 10^{-17}$, $\approx 10^{-17.5}$, $\approx 10^{-18}$ and $\approx 10^{-18.5} \text{ erg cm}^{-2} \text{ s}^{-1}$ for $\text{H}\alpha$, $\text{HeI } 1.08\mu\text{m}$, $[\text{FeII}] 1.64\mu\text{m}$ and $\text{Br}\gamma$, respectively (corresponding to the lower limits of the flux ranges displayed in Fig. 1). The morphologies of the $\text{H}\alpha$ and $\text{HeI } 1.08\mu\text{m}$ emissions, which trace the location of young and massive stars, are rather similar. They exhibit two major peaks along the major axis of NGC 1569, one on each side of the cavities and with the brighter peak located in the North-West (NW) half of the galaxy. Relatively high fluxes are also detected along nearly the full perimeter of the cavities. The $\text{Br}\gamma$ emission is morphologically consistent with that of the $\text{H}\alpha$ although it seems to be relatively weaker along the eastern rim of the cavities. Finally, the $[\text{FeII}] 1.64\mu$ emission, which is typically due to shocks induced by supernova explosions (but see Sect. 5), is as diffuse as the H and He emissions. The $[\text{FeII}]$ flux peaks only in the NW half of NGC 1569 and stays relatively high along the southern rim of the cavities. The very bright compact source in the eastern part of NGC 1569 is a supernova remnant (cf. Labrie & Pritchett 2006).

We integrate the observed $\text{H}\alpha$ and $\text{Br}\gamma$ maps of NGC 1569 over an ellipse of semi-major axis $a = 37''$ (606 pc) and semi-minor axis $b = 17''$ (274 pc) which does not include the extended $\text{H}\alpha$ superbubbles, where shocks due to the galactic outflow seem to be important. The depth of our near-IR imaging is not sufficient to allow us to detect these extended

superbubbles. Pixels below our S/N cut are excluded from the integration.² We use the resulting total H α and Br γ fluxes to derive the color excess (intrinsic + foreground) averaged across the galaxy as in Calzetti et al. (1996):

$$\langle E_g(B - V) \rangle = \frac{-\log(R_{\text{obs}}/R_{\text{int}})}{0.4[\kappa(\lambda_{\text{H}\alpha}) - \kappa(\lambda_{\text{Br}\gamma})]} \quad (1)$$

where R_{obs} is the observed H α /Br γ flux ratio, R_{int} is the intrinsic H α /Br γ flux ratio (102.8) computed for Case B (i.e. the gaseous clouds are optically thick to line photons) assuming a temperature of 10,000 K and a density of 100 cm⁻³ (Osterbrock 1989). The extinction curve $\kappa(\lambda)$ is adopted from Fitzpatrick (1999), with $\kappa(\lambda_{\text{H}\alpha}) = 2.535$ and $\kappa(\lambda_{\text{Br}\gamma}) = 0.363$. We thus obtain $\langle E_g(B - V) \rangle = 0.58$ mag, consistent with Calzetti et al. (1996), and an intrinsic $\langle E_g^i(B - V) \rangle = 0.07$ mag assuming a foreground Galactic color excess $E_G(B - V) = 0.51$ mag (Burstein & Heiles 1982; Calzetti et al. 1996). Since the intrinsic color excess on the stellar continuum is $\langle E_S^i(B - V) \rangle = 0.44 \langle E_g^i(B - V) \rangle$, we estimate the total (intrinsic + foreground) color excess on the stellar continuum to be $\langle E_S(B - V) \rangle = 0.54$ mag, consistent with the values derived by Angeretti et al. (2005) and Grocholski et al. (2008) from the color-magnitude diagram of resolved stars.

We apply Eq. (1) to each pixel in the observed H α and Br γ maps in order to derive the spatial distribution of $E_g(B-V)$ (intrinsic + foreground) across NGC 1569. This is shown in Fig. 2; we clearly see that the color excess is higher (> 0.6 mag) where the H and He emission fluxes are higher, and the NW half of the galaxy is more extinguished than the South-East [where $E_g(B-V) < 0.6$ mag]. The distribution of the pixel color excess as derived from Fig. 2 peaks at about $E_g(B-V) = 0.6$ mag and its full width half maximum

²We compared the resulting total fluxes with those obtained from the same area prior applying ADAPTSMOOTH to find negligible differences, at the 1% - 2% level.

points to variations in $E_g(B-V)$ up to 0.4 mag across the galaxy. The presence of a gradient in $E_g(B-V)$ along the galaxy major axis is evident in Fig. 3, where we plot the azimuthal $E_g(B-V)$ as a function of position along the semi-major axis (solid line; the dotted line represents the foreground $E_G(B-V) = 0.51$ mag). We integrate the observed flux of the $H\alpha$ and $Br\gamma$ images over concentric, elliptical semi annuli and compute the $H\alpha/Br\gamma$ flux ratio to estimate the azimuthal $E_g(B-V)$ as a function of position along the semi-major axis of NGC 1569. From now on, we assume the convention of negative distances for increasing right ascension from the galaxy center. The vertical errorbar (± 0.1 dex) in Fig. 3 indicates the systematic uncertainty on $E_g(B-V)$ due to the uncertainty on the flux calibration. Because of our S/N cut, the color excess can be determined only for galactocentric distances < -50 pc and > 30 pc. As Fig. 3 shows, the color excess increases from $E_g(B-V) \simeq 0.57$ mag in the South-East portion of the galaxy to $E_g(B-V) = 0.7 - 0.8$ mag in the NW. This gradient is consistent with the findings of Kobulnicky & Skillman (1997). The higher $E_g(B-V)$ (~ 0.7) seen at +100 pc from the central cavities in Fig. 3 is in agreement with the findings of González et al. (1997).

We use the 2D spatial map of $E_g(B-V)$ to correct the line-emission images pixel by pixel following the formula:

$$F_i(\lambda) = F_o(\lambda) \times 10^{0.4E_g(B-V)\kappa(\lambda)} \quad (2)$$

where $F_i(\lambda)$ and $F_o(\lambda)$ are the intrinsic and observed line flux, respectively, and $\kappa(\lambda)$ is the extinction law. For a Fitzpatrick's (1999) extinction curve κ is 2.535, 1.096, 0.562 and 0.363 for $H\alpha$, HeI $1.083\mu\text{m}$, [FeII] $1.64\mu\text{m}$ and $Br\gamma$, respectively (Calzetti, private communication). The correction for dust extinction enables us to correct the [FeII] $1.64\mu\text{m}$ emission for the contribution of the Br12 line, estimated to be 0.17 times the $Br\gamma$ flux (assuming Case B, Storey & Hummer 1995). We then compute the surface brightness

profile of NGC 1569 for concentric, elliptical, semi annuli of fixed ellipticity ($b/a = 0.45$) and fixed orientation of the semi-major axis (P.A. = 117°) in each filter. These profiles are shown in Fig. 4 where the surface brightness is corrected for reddening but not for the galaxy inclination. The gap in the line-emission profiles between -50 and 30 pc is due to our S/N cut masking out the central gas-deficient regions. The surface-brightness profiles of the H and He lines share a similar shape, with maxima at a galactocentric distance of about ± 300 pc. At smaller galactocentric distances the surface brightness of the H and He lines declines, while that of the [FeII] line stays constant and is ~ 0.6 dex brighter than $\text{Br}\gamma$. At galactocentric distances < -300 pc and > 300 pc all five profiles are close to an exponential disk with similar scale lengths. All profiles appear to be steeper in the NW half of the galaxy with a typical, exponential scale length of 70 pc against 90 pc as measured for the SE half. The peak at -550 pc in the [FeII] surface brightness is due to the emission from a compact supernova remnant.

4. The recent star formation activity of NGC 1569

We integrate the dereddened $\text{H}\alpha$, HeI $1.08\mu\text{m}$ and $\text{Br}\gamma$ maps of NGC 1569 over an ellipse of semi-major axis $a = 37''$ (606 pc) and semi-minor axis $b = 17''$ (274 pc) which does not include the extended $\text{H}\alpha$ superbubbles. Pixels below our S/N cut are excluded from the integration. We obtain a total, dereddened luminosity of 5.31×10^{40} erg s^{-1} (± 0.20 dex), 4.51×10^{39} erg s^{-1} (± 0.14 dex) and 5.05×10^{38} erg s^{-1} (± 0.11 dex) for the $\text{H}\alpha$, HeI $1.08\mu\text{m}$ and $\text{Br}\gamma$ lines respectively, at the adopted distance of 3.36 Mpc. The quoted uncertainties (all at 1σ level) are due to flux calibration and reddening correction. We use these values to study the stellar population responsible for ionizing the interstellar H and He, and the dereddened $\text{H}\alpha$ and $\text{Br}\gamma$ images to trace the spatial distribution of the SFR density across NGC 1569.

4.1. The recent starburst

We compute the relation between the number of ionizing photons [$Q(\text{H}^0)$] for hydrogen and the $\text{H}\alpha$ ($\text{Br}\gamma$) line luminosity, as well as the relation between the number of ionizing photons [$Q(\text{He}^0)$] for helium and the HeI $1.08\mu\text{m}$ line luminosity, under Case B with a temperature of 10,000 K and a density of 100 cm^{-3} (typical of HII regions):

$$Q(\text{H}^0) [\text{s}^{-1}] = 7.3 \times 10^{11} L(\text{H}\alpha) [\text{erg s}^{-1}] \quad (3)$$

$$Q(\text{H}^0) [\text{s}^{-1}] = 7.5 \times 10^{13} L(\text{Br}\gamma) [\text{erg s}^{-1}] \quad (4)$$

$$Q(\text{He}^0) [\text{s}^{-1}] = 1.0 \times 10^{12} L(\text{HeI } 1.08\mu\text{m}) [\text{erg s}^{-1}] \quad (5)$$

Applying Eq.(3) - (5) to the total, dereddened luminosities from above yields $Q(\text{H}^0) = 3.88 \times 10^{52} \text{ s}^{-1}$ from the $\text{H}\alpha$ line, $Q(\text{H}^0) = 3.79 \times 10^{52} \text{ s}^{-1}$ from the $\text{Br}\gamma$ line, and $Q(\text{He}^0) = 4.51 \times 10^{51} \text{ s}^{-1}$. In Fig. 5 we compare $Q(\text{H}^0)$ (as derived from the $\text{Br}\gamma$ line) and $Q(\text{He}^0)$ with STARBURST99 (Leitherer et al. 1999) predictions for an instantaneous burst of star formation (panel *a*) and for continuous star formation (panel *b*). For both scenarios we adopted $Z = 0.2 Z_{\odot}$ and a Kroupa (2001) initial mass function (with exponents = 1.3 and 2.3 for the mass ranges $0.1 - 0.5 M_{\odot}$ and $0.5 - 100 M_{\odot}$ respectively); stellar evolution was modeled with the Geneva evolutionary tracks for high mass-loss rates (Meynet et al. 1994). In panel *a* of Fig. 5 the correlation between $Q(\text{H}^0)$ and $Q(\text{He}^0)$ for different stellar ages and at fixed total mass (M_{tot}) of the burst is traced by solid lines corresponding to $M_{\text{tot}} = 10^5$, 10^6 and $10^7 M_{\odot}$. The dashed lines represent the correlation between $Q(\text{H}^0)$ and $Q(\text{He}^0)$ for different M_{tot} and at fixed stellar age (1, 3, 5, and 7 Myr). The number of H and He ionizing photons measured for NGC 1569 from its $\text{Br}\gamma$ and $\text{HeI } 1.08\mu\text{m}$ lines is plotted with

a black-filled circle whose errorbars ($\pm 1\sigma$) take into account the systematic uncertainty due to flux calibration and reddening correction. This number is consistent with being produced by a 4 Myr (± 0.3 Myr at 1σ level) old stellar population, comprising ~ 5400 O stars and ~ 250 Wolf-Rayet stars and with a total mass of $1.8 \times 10^6 M_{\odot}$ (with a 20% uncertainty, at 1σ level). In panel *b* the observed values of $Q(\text{H}^0)$ and $Q(\text{He}^0)$ are compared with the predictions for continuous star formation: the solid lines show the correlation between $Q(\text{H}^0)$ and $Q(\text{He}^0)$ at fixed SFR of 0.05, 0.10, 0.15 and 0.20 $M_{\odot} \text{ yr}^{-1}$, and their length spans the time interval between 1 Myr and 1 Gyr. At stellar ages older than 1 Gyr, $Q(\text{H}^0)$ and $Q(\text{He}^0)$ cease to change with time. None of the tracks fits within 1σ the number of H and He ionizing photons measured for NGC 1569; the observed $Q(\text{H}^0)$ and $Q(\text{He}^0)$ are marginally consistent with a star formation history with $\text{SFR} \geq 0.15 M_{\odot} \text{ yr}^{-1}$ that has been going on for more than 10 Myr.

We checked whether the properties of the stellar population ionizing the H and He gas in NGC 1569 vary with galactocentric distance. We integrated the flux of the dereddened $\text{H}\alpha$ and $\text{HeI } 1.083\mu\text{m}$ images over concentric, elliptical semi annuli and derived the corresponding $Q(\text{H}^0)$ and $Q(\text{He}^0)$ as a function of galactocentric distance. We compared these $Q(\text{H}^0)$ and $Q(\text{He}^0)$ values with the SB99 predictions for instantaneous bursts, and found that stellar ages are consistent with a value of ~ 4 Myr at any galactocentric distance. On the other hand, the mass surface density of the ionizing stars increases inward, from $\sim 0.01 M_{\odot} \text{ pc}^{-2}$ at ± 700 pc from the galaxy center to $\sim 0.3 M_{\odot} \text{ pc}^{-2}$ at 300 pc in the SE portion of NGC 1569 and to $\sim 1.8 M_{\odot} \text{ pc}^{-2}$ in the North-West.

4.2. The star formation rate and its density

Using the relation between star formation rate (SFR) and the dereddened $\text{H}\alpha$ (or $\text{Br}\gamma$) luminosity as in Kennicutt (1998) we derive an average SFR of $\simeq 0.4 M_{\odot} \text{ yr}^{-1}$,

consistent with what can be inferred from the age and total mass of the burst derived above. The uncertainty on the flux calibration of both emission lines and on the reddening determination gives rise to a systematic uncertainty of ± 0.20 dex on the SFR derived from the H α (or 0.11 dex on the SFR estimated from the Br γ).

The 2D map of the star formation rate per pixel, obtained from the dereddened Br γ image, is shown in Fig. 6 in logarithmic units; the SFR across NGC 1569 is typically $\simeq 10^{-6}$ M_{\odot} yr $^{-1}$ per pixel (i.e. 3×10^{-7} M_{\odot} yr $^{-1}$ pc $^{-2}$) and increases to few 10^{-5} M_{\odot} yr $^{-1}$ per pixel (i.e. $\simeq 10^{-5}$ M_{\odot} yr $^{-1}$ pc $^{-2}$) at each side of the cavities where the H and He line emissions peak. This trend is well described by the azimuthal SFR density (obtained by integrating the dereddened flux of the Br γ image over concentric, elliptical semi annuli) plotted as a function of position along the semi-major axis (see Fig. 7). The maxima of the SFR density are about 9×10^{-7} M_{\odot} yr $^{-1}$ pc $^{-2}$ and 4×10^{-6} M_{\odot} yr $^{-1}$ pc $^{-2}$ at -300 pc and +300 pc from the galaxy center, respectively. The errorbars ($\pm 1\sigma$) in Fig. 7 indicates a systematic uncertainty of ± 0.1 dex on the SFR derived from the dereddened Br γ image.

The width of the distribution of the pixel star formation rate as obtained from the dereddened Br γ image indicates that SFR density varies by a factor of 10 within the galaxy.

5. The [FeII] emission

The [FeII] emission, with its prominent lines at 1.26 μm and 1.64 μm , is usually explained as triggered by electron collisions occurring in a zone of partially ionized hydrogen where Fe $^{+}$ and e^{-} coexist. The emission intensity is proportional to the size of this region, which is rather small in HII regions but extended in supernova remnants (SNRs, cf. Oliva, Moorwood & Danziger 1989). The [FeII] emission would thus be a clear signpost for SNRs, and as such it is expected to come from compact sources in external galaxies. Recent

studies have shown that the [FeII] emission can also be spatially extended in galaxies known to experience a galactic wind (e.g. NGC 253, Forbes et al. 1993, Sugai, Davies & Ward 2003; NGC 5253, Cresci et al. 2010, Labrie & Pritchett 2006, Turner, Beck & Ho 2000; M 82, Greenhouse et al. 1997, Heckman et al. 1987). Some theoretical computations (e.g. Seab & Shull 1983 and McKee et al. 1987) have shown that this extended [FeII] emission can be explained by high-speed shocks such as those associated with a galactic outflow. The proposed mechanism assumes that iron atoms can be extracted from silicate grains that are preferentially destroyed via nonthermal sputtering and grain-grain collisions (cf. also McCarthy, Heckman & van Breugel 1987; van der Werf et al. 1993. We note that these mechanisms can also be triggered by SN shocks). NGC 1569 is yet another starburst galaxy exhibiting spatially extended emission of [FeII] $1.64\mu\text{m}$ (already detected by Labrie & Pritchett) and a galactic outflow (Heckman et al. 1995).

Given that the $\text{Br}\gamma$ emission comes from gas ionized by OB stars, the flux ratio [FeII] $1.64\mu\text{m}/\text{Br}\gamma$ is commonly used to trace the number ratio of supernovae (SNs) to OB stars, hence the star formation history of a galaxy at fixed initial mass function. Values of this ratio larger than few tens indicate that excitation is mostly produced by SN shocks, while values $\ll 1$, typically 0.1 or lower, are due to photoionization (Alonso-Herrero et al. 1997). The dereddened [FeII] $1.64\mu\text{m}$ luminosity (already corrected for the emission of the Br12 line) integrated over an ellipse of semi-major axis $a = 37''$ and semi-minor axis $b = 17''$ (excluding the central cavities) is $4.67 \times 10^{38} \text{ erg s}^{-1}$ at the adopted distance of 3.36 Mpc. From this and the integrated luminosity of $\text{Br}\gamma$, we obtain a global [FeII] $1.64\mu\text{m}/\text{Br}\gamma$ ratio = 0.9, suggesting that excitation by SN shocks may prevail over photoionization by OB stars formed during the most recent burst. Figure 8 shows the two-dimensional spatial distribution of the [FeII] $1.64\mu\text{m}/\text{Br}\gamma$ ratio across NGC 1569. The line ratio is larger than 1 mainly in the galaxy outskirts and around the central cavities, and it is < 1 especially in two regions at the opposite extremes of the cavities coincident with the peaks of the $\text{H}\alpha$

emission and the star formation rate density. Another way of looking at the spatial variation of the [FeII] $1.64\mu\text{m}/\text{Br}\gamma$ ratio is to integrate the dereddened flux of the [FeII] $1.64\mu\text{m}$ and $\text{Br}\gamma$ images over concentric, elliptical semi annuli and compute the [FeII] $1.64\mu\text{m}/\text{Br}\gamma$ flux ratio as a function of position along the semi-major axis. This is plotted in Fig. 9; the minima at [FeII] $1.64\mu\text{m}/\text{Br}\gamma < 1$ occur at about ± 300 pc from the galaxy center where the star formation rate density is highest (cf. Fig. 8). The peak at -550 pc is due to a compact SNR. The [FeII] $1.64\mu\text{m}/\text{Br}\gamma$ ratio increases above 1 with galactocentric distance and at the edges of the cavities, possibly suggesting that in these regions star formation has been somehow quenched. A relevant caveat on this last interpretation comes from the possibility that iron has been excited by shocks produced by the galactic outflow of NGC 1569. In this case, the [FeII] $1.64\mu\text{m}/\text{Br}\gamma$ ratio may be expected not to trace the star formation history of a galaxy on small spatial scales. The extent by which a galactic outflow can alter this ratio so that it is no longer representative of the local number ratio SNs vs OB stars is still to be thoroughly investigated. In their spectroscopic study of the central $20'' \times 20''$ in NGC 1569 Westmoquette et al. (2007) found little evidence for shocked line ratios, most likely because this area is experiencing intense star formation and photoionization from OB stars. In this region (equivalent to about 320×320 pc² at the adopted distance of 3.36 Mpc) we measure the lowest values of [FeII] $1.64\mu\text{m}/\text{Br}\gamma$ (see Fig. 9, exception made for the cavities edge), which may also be interpreted as due to photoionization.

We used the dereddened, integrated luminosity of the [FeII] $1.64\mu\text{m}$ and $\text{Br}\gamma$ lines to estimate the supernova rate (SNR) and the gas-phase abundance of Fe^+ for NGC 1569 as a whole. Under the assumption that the typical [FeII] $1.64\mu\text{m}$ luminosity of a supernova is $\sim 10^{37}$ erg s⁻¹ and its average life $\sim 10^4$ yr (cf. Lumsden & Puxley 1995), we estimate a SNR of ~ 0.005 yr⁻¹ for the whole galaxy. As for the gas-phase abundance of Fe^+ , we adopt Greenhouse et al.'s (1997) prescription, where:

$$\frac{N(\text{Fe}^+)}{N(\text{H})} \sim 9 \times 10^{-6} \frac{L([\text{FeII}]1.64)}{L(\text{Pa}\beta)} \quad (6)$$

under Case B for a temperature of 10,000 K and a density of 100 cm^{-3} . For the same physical conditions, $L(\text{Pa}\beta) = 5.86 L(\text{Br}\gamma)$, hence:

$$\frac{N(\text{Fe}^+)}{N(\text{H})} \sim 1.54 \times 10^{-6} \frac{L([\text{FeII}]1.64)}{L(\text{Br}\gamma)} \quad (7)$$

We thus derive $N(\text{Fe}^+)/N(\text{H}) \geq 1.4 \times 10^{-6}$ and $N(\text{Fe})/N(\text{Fe})_{\odot} \geq 0.05$, where the Sun $N(\text{Fe})/N(\text{H})$ is 2.8×10^{-5} (Holweger 2001). The lower limit comes from the assumption that all the iron is singly ionized.

6. Conclusions

The wide field of view and high angular resolution of the infrared imager/spectrograph LUCIFER mounted on the Large Binocular Telescope allowed us to acquire deep and detailed images of the local starburst NGC 1569 in the HeI $1.08\mu\text{m}$, [FeII] $1.64\mu\text{m}$ and Br γ light. Together with *HST*/ACS H α images of the galaxy, these data were used to derive the two-dimensional spatial distributions (on scales as small as 2 pc) of dust extinction (foreground + intrinsic), star formation rate density and [FeII] $1.64\mu\text{m}$ /Br γ ratio, and to estimate the age and total mass of the most recent burst responsible for ionizing the interstellar medium (ISM) in NGC 1569. The galaxy looks clearly asymmetric along its major axis with respect to its center, where its super-star clusters A and B have most likely evacuated gas and formed gas-deficient cavities. The color excess $E_g(\text{B-V})$, as derived from the H α /Br γ ratio, is patchy with a scatter of about 0.4 mag across the galaxy. Reddening is lower in the SE portion of NGC 1569 with an average $E_g(\text{B-V}) \simeq 0.57$ mag and increases to 0.7 - 0.8 mag in the NW along the galaxy major axis. Similarly to the surface brightness

profiles of the H and He line emissions, the star formation rate density increases inward along the major axis, reaching two maxima of 9×10^{-7} and $4 \times 10^{-6} M_{\odot} \text{ yr}^{-1} \text{ pc}^{-2}$ at -300 and +300 pc, respectively, from the galaxy center (i.e. just outside the central cavities). Within the galaxy the star formation rate density is seen to vary by a factor of 10. The peaks in SFR density are spatially coincident with the minima in the [FeII] $1.64\mu\text{m}/\text{Br}\gamma$ flux ratio, suggesting that the OB stars formed during the most recent burst are responsible for the ISM photoionization and are preferentially located in a ring around the central cavities. The [FeII] $1.64\mu\text{m}/\text{Br}\gamma$ ratio is seen increasing outward from the galaxy center and along its major axis, as well as at the edges of the central cavities. At face value, this trend may imply that excitation by SN shocks dominates over photoionization from OB stars and indicate that star formation has been quenched some Myrs ago in the central cavities and in the outermost regions of the galaxy. This trend would be consistent with the findings of Aloisi et al. (2001), whereby the age of stars increases with galactocentric distance from 50 Myr close to the galaxy center to >1 Gyr in the galaxy outskirts. How and to which extent the intervention of a galactic outflow as in NGC 1569 alters the [FeII] $1.64\mu\text{m}/\text{Br}\gamma$ ratio and prevents it from tracing the ISM excitation mechanisms on small spatial scales remains to be fully investigated. On global scales, the [FeII] $1.64\mu\text{m}$ luminosity integrated over the galaxy main body points to a SN rate of about 0.005 yr^{-1} and an iron abundance $N(\text{Fe}^+)/N(\text{H}) \geq 1.4 \times 10^{-6}$. This value is quite consistent with the Fe abundance in the ISM of the Small Magellanic Cloud (Rolleston et al. 2003). If the high-speed shocks in the galactic outflow would be responsible for extracting iron atoms from silicate grains (as suggested by the theoretical calculations of, for example, Seab & Shull 1983 and McKee et al. 1987) and hence for a spatially extended [FeII] emission, one would expect to find the ISM Fe abundance in NGC 1569 to be enhanced with respect to the Small Magellanic Cloud (SMC) which has a stellar metallicity similar to NGC 1569 but no galactic outflow. Given that the ISM Fe abundance is similar in both NGC 1569 and the SMC, the present

data would tend to exclude that the diffuse [FeII] emission in NGC 1569 is due to the galactic outflow. Moreover, Sofia et al. (2006) found that iron atoms in the ISM of the SMC are most likely locked in metal grains and/or oxides rather than in silicates. If this applied to NGC 1569 also, the galactic outflow would not be able to extract iron from dust grains (as in the scenario proposed by Seab & Shull 1983 and McKee et al. 1987), increase the Fe emission and thus explain its spatial extension.

We used the $H\alpha$, $Br\gamma$ and HeI $1.08\mu\text{m}$ luminosities integrated over NGC 1569 to estimate the star formation rate of the most recent burst ($\simeq 0.4 M_{\odot} \text{ yr}^{-1}$) and the number of stellar photons able to ionize the interstellar H and He gas [i.e. $Q(H^0)$ and $Q(He^0)$]. When compared to STARBURST99 predictions the observed $Q(H^0)$ and $Q(He^0)$ enable us to constrain the age and the mass of the stellar population responsible for ionizing H and He. In the case of NGC 1569 the values of $Q(H^0)$ and $Q(He^0)$ are in good agreement with an instantaneous burst of star formation. A scenario where star formation is continuous and takes place with a constant SFR is not rejected by statistics, but is seemingly inconsistent with the gasping nature of the star formation activity undergone by NGC 1569 in the last 1 Gyr, as derived by Angeretti et al. (2005) from the color-magnitude diagram of resolved stars. The best-fitting instantaneous burst occurred about 4 Myr ago and involved a total stellar mass of $\simeq 1.8 \times 10^6 M_{\odot}$. It gave birth to about 5400 O stars and 250 Wolf-Rayet stars. Such a stellar age is constant with galactocentric distance and where $H\alpha$, $Br\gamma$ and HeI $1.08\mu\text{m}$ emissions are detected. The only property of the burst changing with distance from the galaxy center is the surface mass density of the ionizing stars, which follows the surface brightness profiles of the H and He lines and increases from $\sim 0.01 M_{\odot} \text{ pc}^2$ in the galaxy outskirts up to $\sim 1.8 M_{\odot} \text{ pc}^2$ just outside the central cavities. The comparison of this latest starburst with the three episodes of star formation identified by Angeretti et al. (2005, cf. Sect. 1) suggests a star formation history where the burst duration and average SFR have become shorter and larger, respectively, from 1 Gyr ago to 4 Myr ago. Consequently, the

total mass in stars produced by these bursts of star formation has decreased by a factor of about 20 in the last 1 Gyr. Interestingly enough, the 4 Myr age derived from the observed $Q(\text{H}^0)$ and $Q(\text{He}^0)$ is close to that of the younger stellar component found mostly in SSC A by González Delgado et al. (1997). Therefore, the big picture emerging from these results is one where the strong stellar winds and supernova explosions from the older stellar population of SSCs A and B (about 9 Myr old) removed a large fraction of gas from the clusters surroundings and triggered, ~ 4 Myr later, star formation at the edges of the central cavities. The gas left over in the vicinity of SSC A (and perhaps also B) underwent star formation nearly at the same time.

We would like to thank Daniela Calzetti and Monica Tosi for very useful discussions. The Dark Cosmology Centre is funded by the DNRF.

Facilities: LBT (LUCIFER), HST (ACS)

REFERENCES

- Ageorges, N., et al., 2010, Proc. SPIE, 7735, 77351L
- Aloisi, A., et al., 2001, ApJ, 121, 1425
- Alonso-Herrero, A., Rieke, M.J., Rieke, G.H., & Ruiz, M., 1997, ApJ, 482, 747
- Angeretti, L., Tosi, M., Greggio, L., Sabbi, E., Aloisi, A., & Leitherer, C., 2005, AJ, 129, 2203
- Arp, H., & Sandage, A., 1985, MPA Rep., 173, 29
- Broadhurst, T., Ellis, R., & Glazebrook, K. 1992, Nature, 355, 55
- Burstein, D., & Heiles, C., 1982, AJ, 87, 1165
- Calzetti, D., Kinney, A., & Storchi-Bergmann, T., 1994, ApJ, 429, 582
- Calzetti, D., Kinney, A., & Storchi-Bergmann, T., 1996, ApJ, 458, 132
- Cole, S., Aragón-Salamanca, A., Frenk, C.S., Navarro, J.F., & Zepft, S.E. 1994, MNRAS, 271, 781
- Cresci, G., Vanzi, L., Sauvage, M., Santangelo, G., & van der Werf, P., 2010, submitted to A&A, arXiv:1007.3666
- De Marchi, G., Clampin, M., Greggio, L., Leitherer, C., Nota, A., & Tosi, M., 1997, ApJ, 479, L27
- Fitzpatrick, E.L., 1999, PASP, 111, 63
- Forbes, D., Ward, M.J., Rotaciuc, V., Blietz, M., Genzel, R., Drapatz, S., van der Werf, P.P., & Krabbe, A., 1993, ApJ, 406, L11

- González Delgado, R.M., Leitherer, C., Heckman, T., & Cerviño, M., 1997, *ApJ*, 483, 705
- Greenhouse, M.A., et al., 1997, *ApJ*, 476, 105
- Greggio, L., Tosi, M., Clampin, M., De Marchi, G., Leitherer, C., Nota, A., & Sirianni, M., 1998, *ApJ*, 504, 725
- Grocholski, A.J., et al., 2008, *ApJ*, 686, L79
- Heckman, T.M., Armus, L., McCarthy, P., van Breugel, W., & Miley, G.K., 1987, in *Star formation in galaxies*. ed. C.J. Lonsdale Persson, p. 461 (N87-24266 17-89)
- Heckman, T.M., Dahlem, M., Lehnert, M.D., Fabbiano, G., Gilmore, D., & Waller, W.H., 1995, *ApJ*, 448, 98
- Hill, J.M., Green, R.F., & Slagle, J.H., 2006, *Proc. SPIE*, 6267, 62670Y
- Ho, L.C., & Filippenko, A.V., 1996, *ApJ*, 466, L83
- Holweger, H., 2001, in *Solar and Galactic Composition: A Joint SOHO/ACE Workshop*, AIP Conference Proceedings, 598, 23
- Hunter, D.A., Hawley, W.N., Gallagher, J.S., III, 1993, *AJ*, 106, 1797
- Izotov, Y.I., & Thuan, T.X. 1999, *ApJ*, 511, 639
- Kauffmann, G., White, S.D.M., & Guiderdoni, B. 1993, *MNRAS*, 264, 201
- Kennicutt, R.C., Jr., 1998, *ARA&A*, 36, 189
- Kobulnicky, H.A., & Skillman, E.D., 1997, *ApJ*, 489, 636
- Kroupa, P., 2001, *MNRAS*, 322, 231
- Labrie, K., & Pritchett, C.J., 2006, *ApJS*, 166, 188

- Leitherer, C., et al., 1999, *ApJS*, 123, 3
- Lilly, S.S.J., Tresse, L., Hammer, F., Crampton, D., & Le Fevre, O., 1995, *ApJ*, 455, 108
- Lumsden, S.L., & Puxley, P.J., 1995, *MNRAS*, 276, 723
- Martin, C.L., 1998, *ApJ*, 506, 222
- McCarthy, P.J., Heckman, T.M., & van Breugel, W., 1987, *AJ*, 93, 264
- McKee, C.F., Hollenbach, D.J., Seab, C.G., & Tielens, A.G.G.M., 1987, *ApJ*, 318, 674
- Meurer, G., 1995, *Nature*, 375, 742
- Meurer, G., Heckman, T.M., Leitherer, C., Kinney, A., Robert, C., & Garnett, D., 1995, *AJ*, 110, 2665
- Meynet, G., Maeder, A., Schaller, D., & Charbonnel, C., 1994, *A&AS*, 103, 97
- Moustakas, J., & Kennicutt, R.C., Jr, 2006, *ApJS*, 164, 81
- Oliva, E., Moorwood, A.F., & Danziger, I.J., 1989, *A&A*, 214, 307
- Origlia, L., Leitherer, C., Aloisi, A., Greggio, L., & Tosi, M., 2001, *AJ*, 122, 815
- Osterbrock, D.E., 1989, *Astrophysics of Gaseous Nebulae and Active Galactic Nuclei*,
University Science Books: Mill Valley, California
- Reakes, M., 1980, *MNRAS*, 192, 297
- Rolleston, W.R.J., Venn, K., Tolstoy, E., & Dufton, P.L., 2003, *A&A*, 400, 21
- Seab, C.G., & Shull, J.M., 1983, 275, 652
- Seifert, W., et al., 2010, *Proc. SPIE*, 7735, 77357W

- Stil, J.M., & Israel, F.P., 1998, *A&A*, 337, 64
- Storey, P.J., & Hummer, D.G., 1995, *MNRAS*, 272, 41
- Sugai, H., Davies, R.I., & Ward, M.J., 2003, *ApJ*, 584, 9
- Turner, J.L., Beck, S.C., & Ho, P.T.P., 2000, *ApJ*, 532, 109
- Vallenari, A., & Bomans, D.J., 1996, *A&A*, 313, 713
- van den Bergh, S., 1995, *Nature*, 374, 215
- van der Werf, P.P., Genzel, R., Krabbe, A., Blietz, M., Lutz, D., Drapatz, S., Ward, M.J.,
& Forbes, D.A., 1993, *ApJ*, 405, 522
- Waller, W.H., 1991, *ApJ*, 370, 144
- Westmoquette, M.S., Smith, L.J., & Gallagher, J.S., III, 2008, *MNRAS*, 383, 864
- Westmoquette, M.S., Smith, L.J., Gallagher, J.S., III, & Exter, K.M., 2007, *MNRAS*, 381,
913
- White, S.D.M., & Frenk, C.S. 1991, *ApJ*, 379, 52
- Whitmore, B.C., et al., 1993, *AJ*, 106, 1354
- Zibetti, S., 2009, submitted to *MNRAS* (arXiv0911.4956)
- Zibetti, S., Charlot, S., & Rix, H.-W., 2009, *MNRAS*, 400, 1181

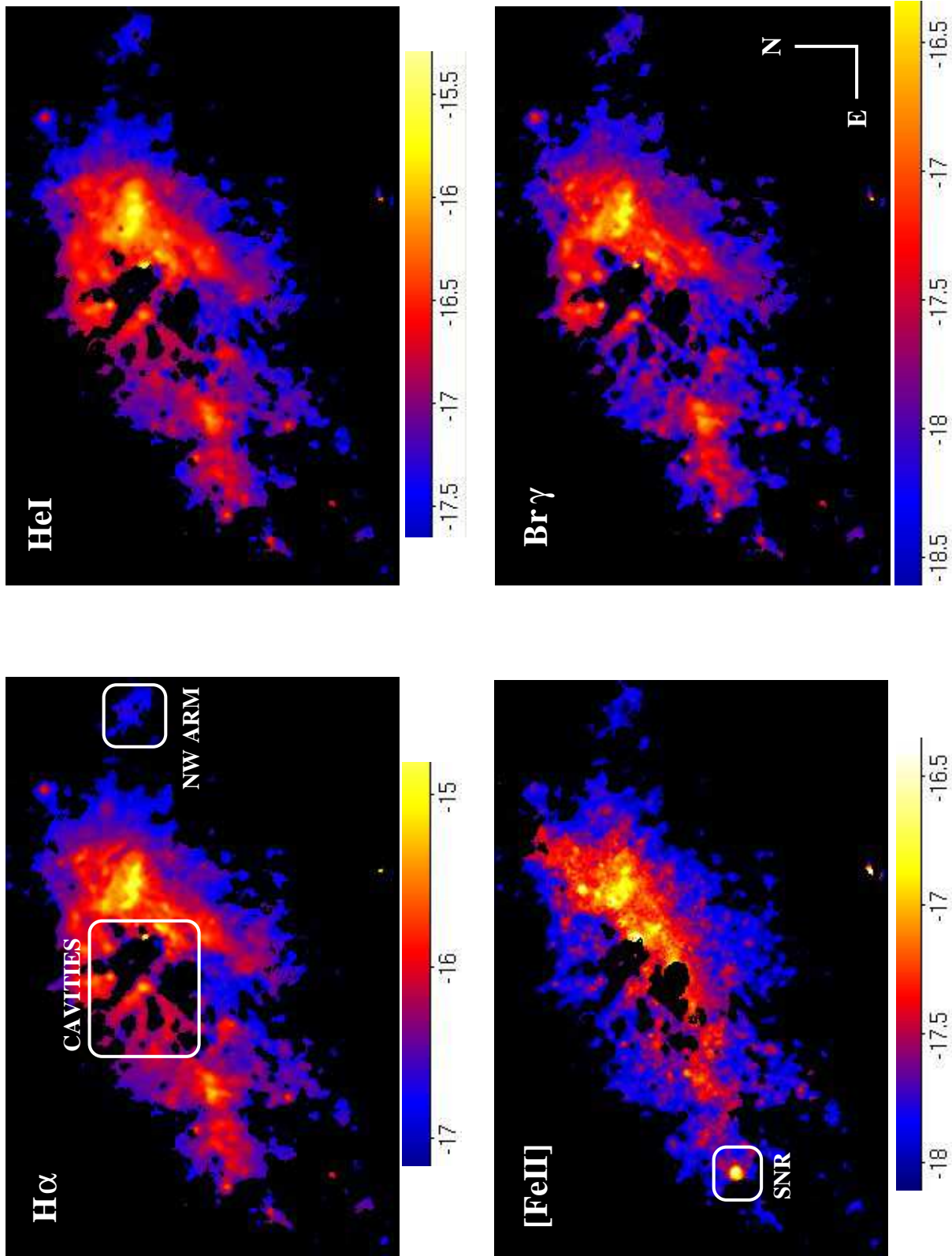


Fig. 1.— The line-emission images of NGC 1569 calibrated in flux in units of $\text{erg cm}^{-2} \text{s}^{-1}$, but not corrected for reddening. Fluxes are on logarithmic scale, and the image size is $1.5 \text{ kpc} \times 1 \text{ kpc}$ at the adopted distance of 3.36 Mpc. The white frames indicate the location of

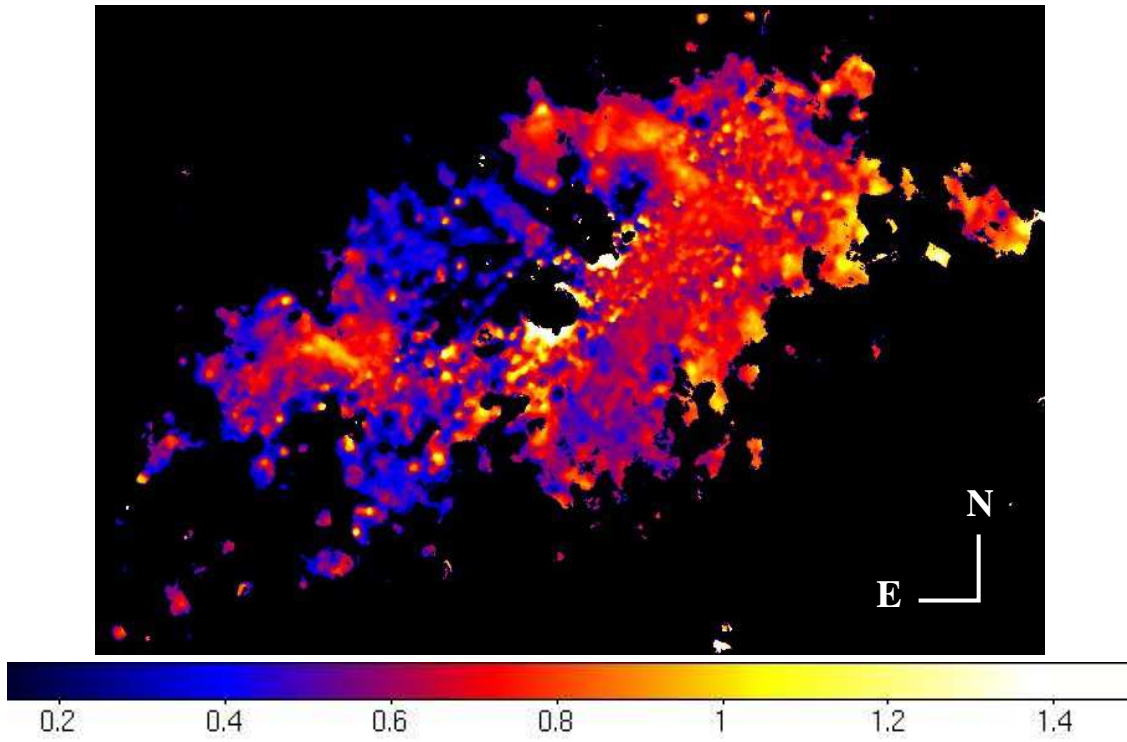


Fig. 2.— The $E_g(B-V)$ (intrinsic + foreground) map of NGC 1569 derived from the $H\alpha/Br\gamma$ flux ratio. The image size is $1.5 \text{ kpc} \times 1 \text{ kpc}$.

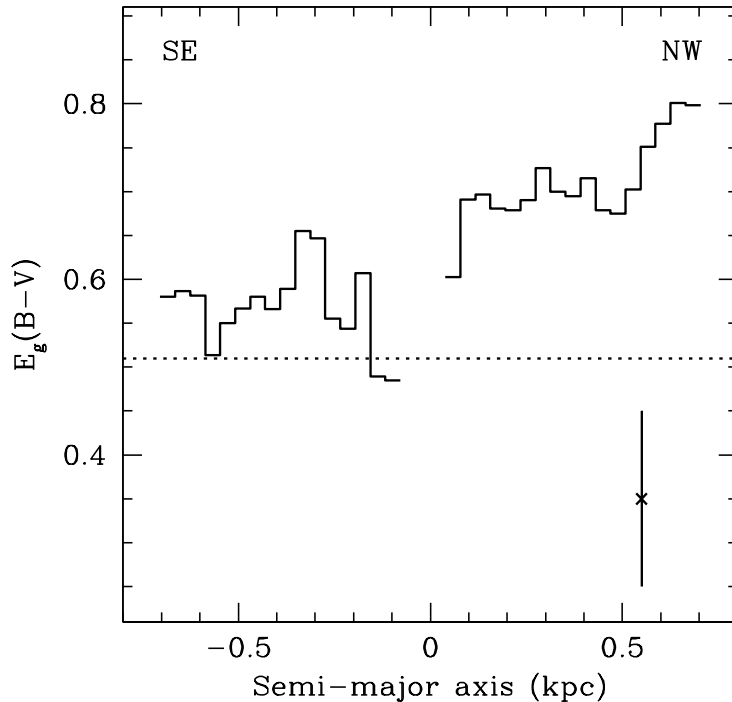


Fig. 3.— The azimuthal $E_g(B-V)$ (intrinsic + foreground), computed over 180 degrees, as a function of position along the semi-major axis (solid line). The dotted line represents the foreground Galactic color excess in the direction of NGC 1569, $E_G(B-V) = 0.51$ mag. The errorbar corresponds to a systematic uncertainty on $E_g(B-V)$ of ± 0.1 mag, and is due to the uncertainty on the flux calibration. The gap between -50 and 30 pc is due to our S/N cut which masked out the central, gas-deficient regions.

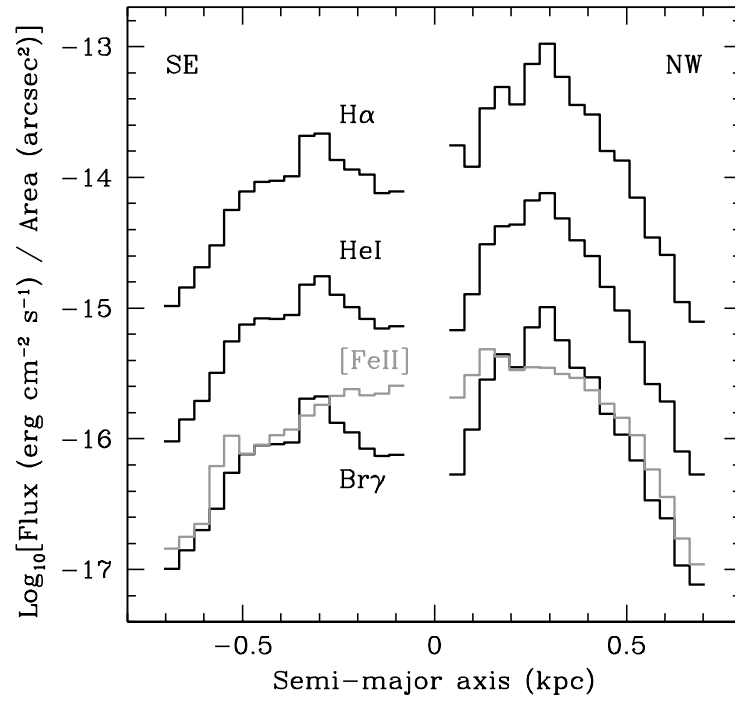


Fig. 4.— The surface brightness profile of NGC 1569 in the different narrow-band filters. Fluxes are corrected for $E_g(B-V)$. The gap between -50 and 30 pc is due to our S/N cut which masked out the central, gas-deficient regions.

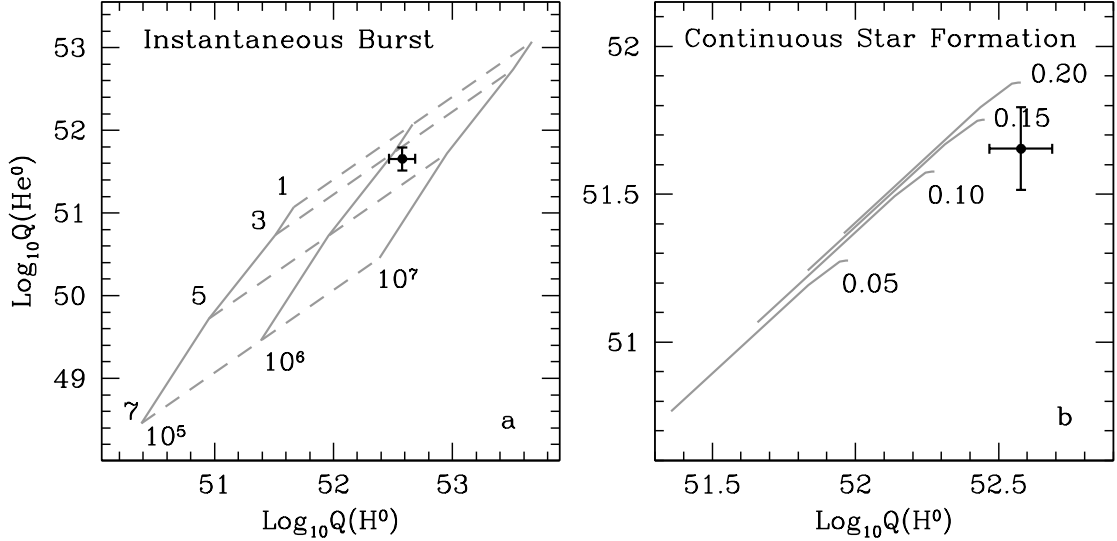


Fig. 5.— *Panel a*: the number of photons ionizing He [$Q(\text{He}^0)$] is plotted as a function of the number of photons ionizing H [$Q(\text{H}^0)$] as derived from the $\text{Br}\gamma$ line. The solid lines trace the correlation between $Q(\text{H}^0)$ and $Q(\text{He}^0)$ at fixed total mass of the burst (10^5 , 10^6 and $10^7 M_\odot$) and as a function of age (1, 3, 5, 7 and 10 Myr). The dashed lines show the correlation between $Q(\text{H}^0)$ and $Q(\text{He}^0)$ at fixed age and as a function of total mass of the burst. The black-filled circle represents the $Q(\text{H}^0)$ and $Q(\text{He}^0)$ values measured for NGC 1569 in this work. The errorbars are $\pm 1\sigma$. *Panel b*: as before, but the solid lines here trace the predictions for a continuous star formation with different star formation rates (0.05, 0.10, 0.15 and $0.20 M_\odot \text{ yr}^{-1}$). The line length corresponds to a time interval between 1 Myr (bottom left corner of each line) and 1 Gyr (top right corner); for ages older than 1 Gyr $Q(\text{H}^0)$ and $Q(\text{He}^0)$ remain unchanged.

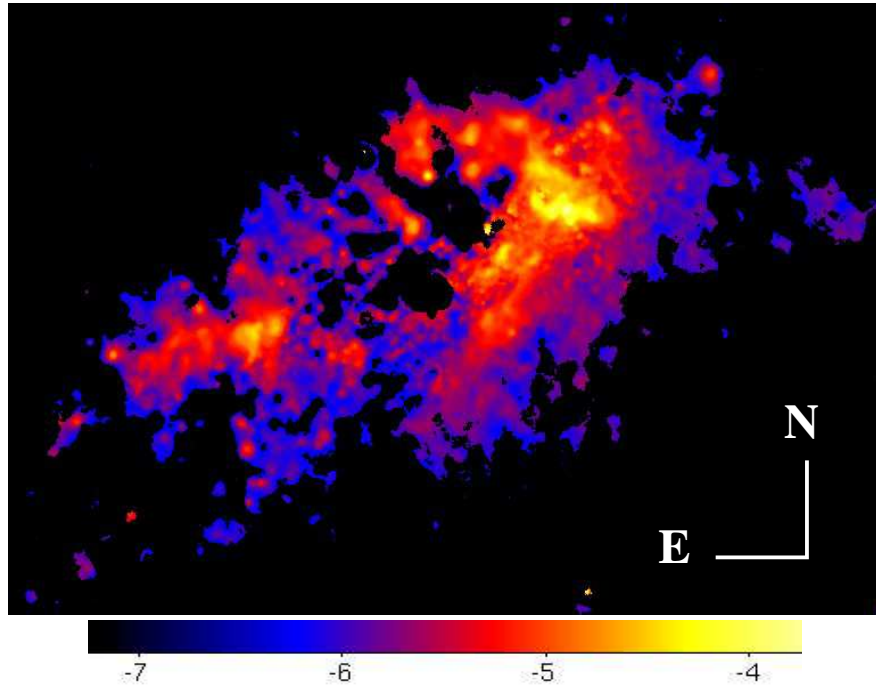


Fig. 6.— The star formation rate map of NGC 1569 derived from the dereddened Br γ image. The image size is 1.5 kpc \times 1 kpc. The star formation rate is in units of $M_{\odot} \text{ yr}^{-1}$ per pixel, and is displayed on logarithmic scale.

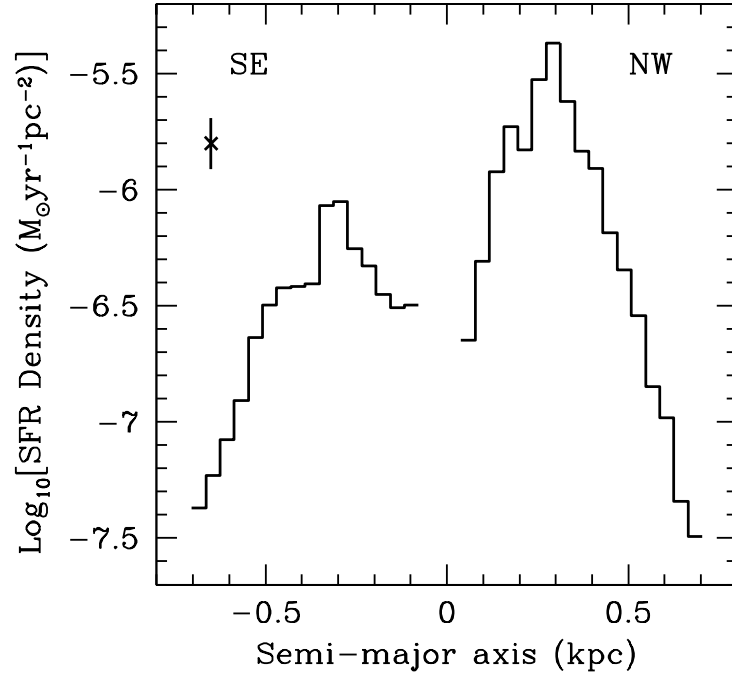


Fig. 7.— The azimuthal SFR density as a function of position along the semi-major axis, obtained from the dereddened Br γ image. The errorbar (± 0.11 dex) represents the systematic uncertainty on SFR due to the uncertainty on the flux calibration and color excess. The gap between -50 and 30 pc is due to our S/N cut which masked out the central, gas-deficient regions.

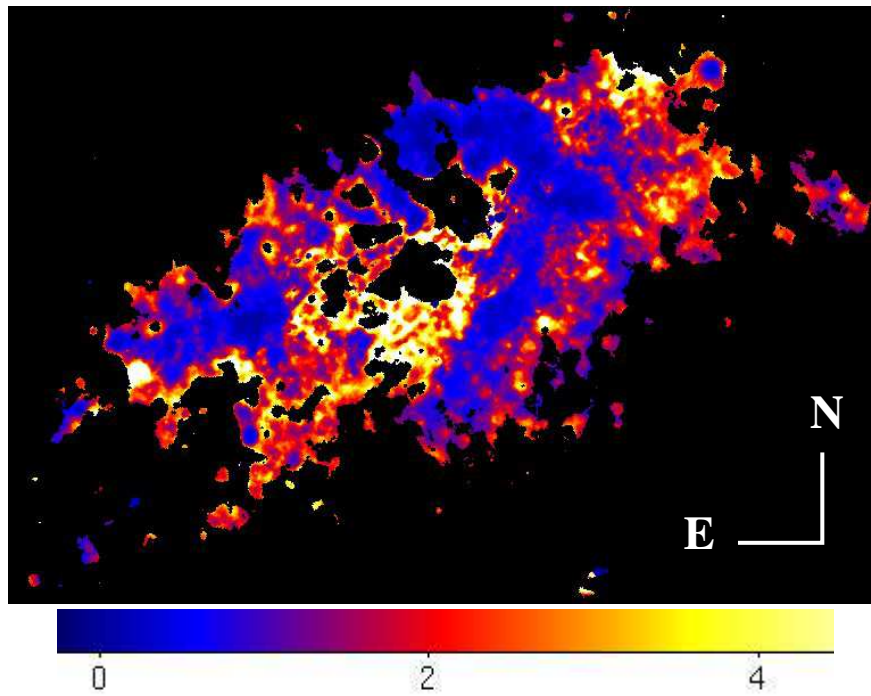


Fig. 8.— The 2D map of the [FeII] $1.64\mu\text{m}/\text{Br}\gamma$ flux ratio, after correction for reddening. The image size is $1.5 \text{ kpc} \times 1 \text{ kpc}$.

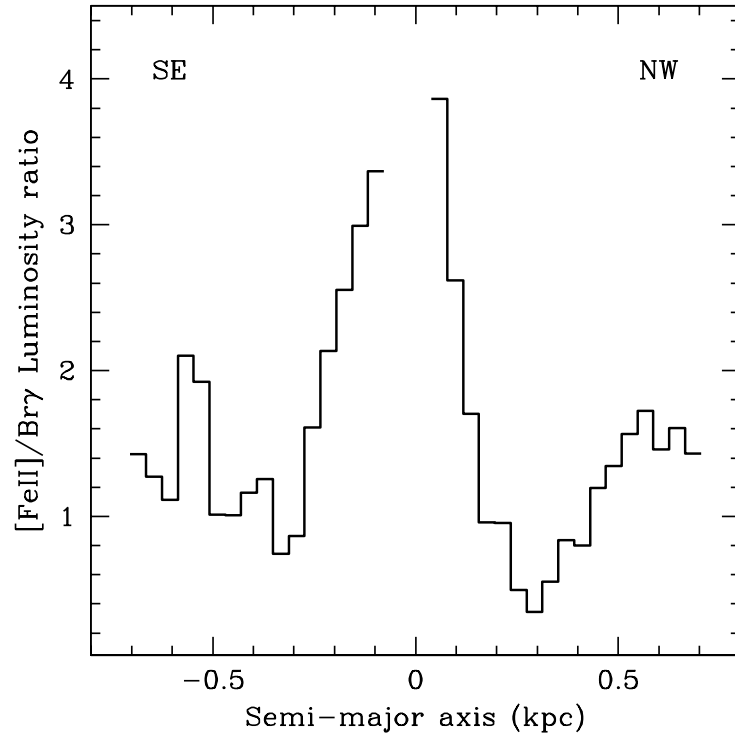


Fig. 9.— The azimuthal [FeII] $1.64\mu\text{m}/\text{Br}\gamma$ flux ratio, corrected for reddening, as a function of position along the semi-major axis. The gap between -50 and 30 pc is due to our smoothing procedure which masked out the central, gas-deficient regions.

Table 1: Near-IR and optical total exposure times on source

Filter	Exposure Time (min)
J	20
H	55
K	121
HeI $1.08\mu\text{m}$	30
[FeII] $1.64\mu\text{m}$	67
Br γ	111
F606W	326
F658N	77